JME

Journal of Mining & Environment,
Vol.2, No.2, 2011, 126-135.

Limestone chemical components estimation using image processing and pattern recognition techniques

F. Khorram[1], H. Memarian[2*], B. Tokhmechi[3], H. Soltanian-zadeh[4]

1. M.Sc student, Mineral Exploration Engineering, School of Mining, College of Engineering, University of Tehran
2. Professor of Geo-Engineering, School of Mining, College of Engineering, University of Tehran
3. Assistant professor of Mining Engineering, Faculty of Mining, Petroleum and Geophysics, Shahrood University of Technology
4. Professor of Electrical Engineering, School of Electrical and Computer, College of Engineering, University of Tehran

Received 20 Sep 2011; received in revised form 20 Dec 2011; accepted 9 March 2012
*Corresponding author: memarian@ut.ac.ir (H. Memarian).

Abstract
In this study, an ore grade estimation model was developed based on image processing and pattern recognition techniques. The study was performed at a limestone mine in central part of Iran. The samples were randomly collected from different parts of the mine and crushed down (from 10 cm to 2.58 cm). The images of the samples were taken in an appropriate environment and processed. A total of 76 features were extracted from the identified rock samples in all images. Neural network was used as an intelligent tool for ore grade estimation. First, six principal components derived from principal component analysis were used as input of neural network and four grade attributes of limestone ($CaCO_3$, Al_2O_3, Fe_2O_3 and $MgCO_3$) were used as the output. The root of mean squared error between the observed values and the model estimated values for the test data set were 0.38, 0.84, 0.15 and 0.03; the R2 values were 0.78, 0.76, 0.76 and 0.81 for the mentioned chemical compositions respectively. The value of R_2 indicates the correlation between the actual and estimated data. It can therefore be inferred that the model could successfully estimate the percentage of chemical compositions of the samples collected from the same mine.

Keywords: *Image processing; neural network; ore grade; prediction; limestone*

1. Introduction

Vision-based systems have great success in the mineral industries [1]. A study conducted by Oestreich et al. (1995) demonstrated the use of an online sensor for mineral composition identification [2]. Petruck and Lastra (1993) have determined mineral grade values on a microscopic scale by image processing technique [3]. Shafarenko et al. (1997) used an image-based technique to inspect the quality of granitic rocks [4]. Casali et al. (2000) carried out an ore grind-ability analysis based on vision systems [5]. Ore textural analysis using the image processing techniques was performed by several investigators [6, 8]. The main scope of these studies was to estimate average particle size and various ore type identification in the industrial ore feeding systems [9].

In most cases, the ore grades are determined by manually collecting samples from ore material and analyzing them chemically in a laboratory. The sample collection, preparation and chemical analysis are tedious and time-consuming operations. In this situation, a vision sensor might be a useful technology for grade quality control [10]. Chatterjee et al (2006) developed a vision system based on a neural network that was trained by the image features to estimate the grade of chemical compositions in a limestone mine [10]. In this paper, the effects of different combination of image features on the chemical grade determination were considered. Schematic

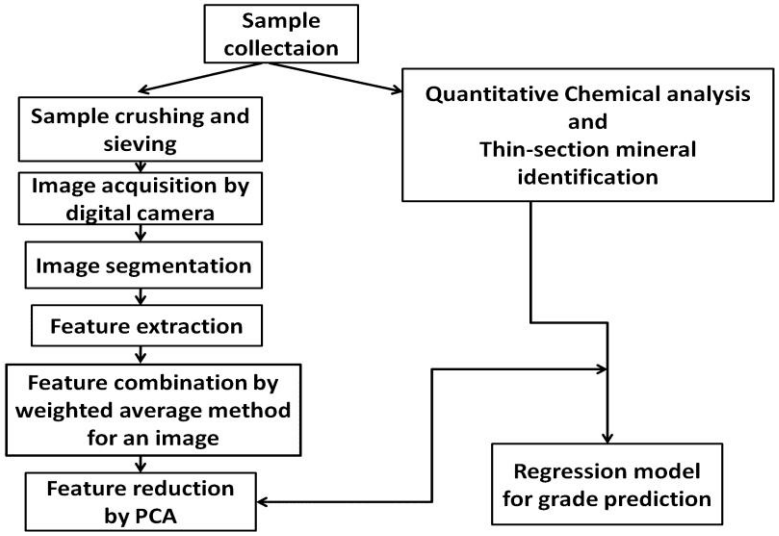

Figure1. A schematic diagram showing the stages of the image processing based grade estimation

diagram of the methodology applied in this study is shown in Figure 1.

2. Methodology

2.1. Image processing

One of the critical phases in image processing is an appropriate acquisition of the images. The images should be taken in a controlled and stable environment to avoid the influences of extraneous factors. Several preprocessing algorithms are available for removing unwanted noise and other artifacts produced in images during their acquisition. The average and the median filters are suitable for noise reduction in the images [11]. The median filter can especially eliminate the effect of high magnitude noises. In this study, a median filter has been applied, which sorts the pixels in a 8×8 region and replaces the central pixel with the median value.

Image segmentation is a technique that subdivides an image into its constituent regions or objects. The level to which the subdivision is carried out depends on the goal of the segmentation process [11, 14]. The manual digitization technique is one of the easiest image segmentation techniques, but it is tedious and time-consuming. Graham et al. (2005) suggested that no single image segmentation technique is perfect for segmenting the grain samples from their neighbors [15]. A particular segmented region might contain more than one rock sample. Thus, individual rock samples should be identified with labels from the segmented image.

For object identification, a region labeling algorithm has been used [16]. Typically, a region labeling algorithm examines each pixel in a mapping, and compares its value to those of its neighbors. If the pixel value is close enough to its neighboring values, then it is assumed to be in the same region as those of the neighbors. For the use of a regional labeling algorithm, a binary image is scanned from the top left to the bottom right. The first object pixel (i, j) encountered in the image is assigned a unique label. This label value is propagated and the region is grown to those pixels, which possess the same pixel value as that of the (i,j) pixel using the 8-neighbours connectivity method [14]. In the next step, the eight neighbors of those previously labeled pixels are examined and those which have the same pixel value are labeled.

After the regional labeling, the original gray values of the labeled objects are then superimposed on the segmented images so that each object has its original gray value with the background value set to zero [17]. The rock samples properties in the image are described by various features. Therefore, the next step of the image processing is to extract different features from the individual objects. The features are characterized by three categories: color, morphology and texture. One of the most important properties for distinguishing limestone is its color [18]. The color feature is characterized by the intensity levels of its seven color components, namely r, g, b, H, S, I, and gray [11].

The texture and morphology features of lime stones vary with the depositional variability and weathering of the limestone beds [18]. For example, for the limestone mine under investigation, it has been observed that the shape of Dolomitic limestones become somewhat

spherical after blending, but pure limestone obtains an elongated shape after crushing. It is very likely that, if these features are extracted and mapped with proper modeling, then they might have some relationships with rock type properties as well as their grades [10].

In order to calculate the features of an image, assume that the number of distinct rock objects in an image is n and the numbers of features extracted from each rock chips is M. Then, the feature value xi for that image is calculated by the weighted average of different rock object features present in the image.

$$x_i = \sum_{j=1}^{n} w_j \, x_{ij} \qquad (1)$$

$$w_j = \frac{a_j}{\sum_{j=1}^{n} a_j}$$

where j=1,2,…,n; i=1,2,….,M, X_{ij} is the ith feature of jth rock object from a given image. a_j is the number of pixel in the rock object j.

2.2. Feature vector reduction

The large number of extracted features yields a high-dimensional feature vector. In addition, some of these features might be correlated with each other. High-dimensional feature vector might cause redundancy in data analysis. The redundant features can be discarded with preserving important information by the use of dimension reduction techniques on the feature vector. The dimension reduction techniques employed in this study is the Principal Component Analysis PCA [22]. Principal Component Analysis (PCA) is one of the most widely used methods for reducing the dimension of a multivariate data set. It transforms a group of correlated features into the principal components (PC_s), using a linear transformation. It is possible to extract as many PC_s as the number of features, in the feature vector. Then PC_s are orthogonal and are sorted based on their variance quantity in descending order successively. The variances of the last few PC_s do not have a significant contribution to the total data variance, and can be eliminated. Therefore PCA is an effective means for reducing the dimensionality of feature vectors.

2.3. Neural network for ore grade modeling

In this research an attempt has been made to find out the relationship between various image-based rock features with the grades, using neural network techniques. Estimation of ore grades is carried out using the feature vectors (after dimension reduction) as inputs to a neural network model that defines the relationship between ore grades and feature vectors.

Artificial neural network is a modeling tool with the ability to learn the complex inter-relationship between the input and the output variables of multi-dimensional data [23, 25]. The multi-layer perceptron neural network MLP model is a popular model that has been used in this study. During the learning phase, the network is learned with a group of known image features and grade values. Using an optimal learning algorithm, the connection weights that connect the neurons of different layers are modified iteratively. After some iteration, they become adjusted in such a way that when the input image features are presented, the network produces grade outputs, which are close to their actual output values. Detailed descriptions of neural networks are beyond the scope of this paper. The reader is referred to proper references [23, 25].

The Levenberg-Marquardt algorithm was used for error minimization. The learning basically starts with an untrained network, presents a training data (here PCs of image features) to the input layer, passes the signals through the network, and determines the output (grade attributes) at the output layer. These outputs are compared with the target values and any observed differences between these two correspond to an error. The error value is a function of the weights and is minimized when the network outputs match the desired output. The weights are thus adjusted to reduce this measure of error. The error on a pattern is given by:

$$E(w) = \frac{1}{2}\sum_{k=1}^{c}(t_k - z_k)^2 \qquad (2)$$

$$= \frac{1}{2} \, |t - z|^2$$

where t and z are the actual grades and the network output grades, and c is the number of grade attributes. The weights are initialized with random values, and are then changed in a direction that will reduce the error [23]. The Levenberg-Marquardt algorithm is a very simple, but robust method for approximating a function. Basically, it consists in solving the equation:

$$(J_t J + \lambda I)\delta = J_t E \qquad (3)$$

where **J** is the Jacobean matrix for the system, **λ** denotes the Levenberg's damping factor, **δ** represents the weight update vector that we want to find and **E** is the error vector containing the output errors for each input vector used on training the network. The **δ** tells us that how much we should change our network weights to achieve a better solution. The $\mathbf{J}_t\mathbf{J}$ matrix can also be

known as the approximated Hessian. The **λ** damping factor is adjusted at each epoch, and guides the optimization process. If reduction of **E** is rapid, a smaller value can be used, whereas if an epoch gives insufficient reduction in the residual, **λ** can be increased.

The Jacobean is a matrix of all first-order partial derivatives of a vector-valued function. In the neural network case, it is an **N**-by-**W** matrix, where **N** is the number of entries in our training set and, **W** is the total number of parameters (weights + biases) of our network. It can be created by taking the partial derivatives of each output in respect to each weight. In traditional Levenberg-Marquardt implementations, the Jacobean is approximated using finite difference approximation technique. However, for neural network, it can be computed very efficiently using the chain rule of calculus and the first derivatives of the activation functions. Hence, the adjusted weights are used to calculate the error term for the next iteration. The process is repeated in the same manner and stopped when the error reaches a threshold value. After completion of the training, the model can be used for estimation purposes. One of the critical aspects of neural network modeling is the development of a generalized model. The generalization is defined as applicability of a model for the data sets except training data. The neural network model is very flexible and, therefore, powerful enough to capture any complex relationship between the input and the output variables [24]. A neural network modeler always tries to build up a generalized model with a given data set. A model calibration exercise is a good practice to obtain generalized model [24].

3. Case study

3.1. Data collection

The study was carried out in a limestone mine situated in the central part of Iran. The mine is located in Southeast of the Shahmirzad and East of the Darband in the Semnan province. Soltanieh formation consisting dark gray dolomite with thin bedded limestone and Elica Formation with light gray limestone exposed in different parts of the studied mine. Altogether 30 samples were collected from different parts of the mine. The samples weighed approximately 5 kg, and the size range varied from 25 to 30 cm. After sample collection, they were crushed with Jaw crusher and sieved. The 2.58-10 cm fraction was selected and examined.

The percentage of $CaCO_3$, Al_2O_3, Fe_2O_3, and $MgCO_3$, were determined using Titration method for all the rock samples. In addition, the rocks' thin sections were studied under polarization microscope to identify the type of minerals. All of samples consisted of dolomite, calcite and their compositions. No other minerals were found in thin sections. Table 1 illustrates the range of chemical composition percentage, and the type of rock samples from the lithological composition point of view regarding their macroscopic visual features.

Table 1. Percentage of chemical composition and lithological description

		limestone	Dolomitic limestone	Dolomitic mixed high calcium limestone
Lithological Description		-Micro crystalline -Massive -Obvious calcite veins -Obvious veins filled with solid solutions -Light Milk-White, pink and gray in color	-Coarse crystalline -Porous -Brittle -Dark gray with dark brown and red spots	-Micro crystalline -Slightly porous -Brittle -Milk-whit and dark gray with gray and brown spots
Chemical composition	$CaCO_3$	80-98%	42.8 -57%	57.7 -62.4%
	Fe_2O_3	0.05-0.28%	0.19 -0.45%	0.16 -0.27%
	Al_2O_3	0.06 -0.96%	0.13 -1.25%	0.23 -0.9%
	$MgCO_3$	0.84 -17.22%	41.16 -54%	36.12 -40.32 %

3.2. Image acquisition

To avoid the influences of extraneous factors an identical condition is developed for image acquisition in this work. The image acquisition system consists of four wooden plates, two 9Watt lamps as illumination system, a digital camera (DMC-LC 50 Panasonic) and a computer. Since the lighting type, the location and the color quality are crucial for clear images, uniform diffuse lighting was used. The wooden plates were placed at 40 cm distance at the four sides of considered samples. The camera was placed in a stable 30 cm distance from the samples. The distance of lamps was 25 cm in all images. Two successive images for each sample were taken by changing the

placement and the orientation of the rock samples. The changing of position and orientation of the rock samples was done for two basic reasons. Firstly, if images are taken from one side of the rocks, extracted features may not be the true representative of the rock samples. Therefore by taking the images from different positions of rock samples, the generalization capability of extracted features will increase [10]. The size of images is 2080×11544 and local resolution of images is 0.15 mm /pixel.

3.3. Image analysis of the samples

After image acquisition the images were processed. As explained in 2.2, the preprocessing was carried out with a 8×8 median filter. In order to identify discrete regions representing rock samples, a hybrid segmentation technique was proposed. Figure 2 shows the different steps involved in segmentation technique. The theoretical discussion of the techniques is outside the scope of this paper. Interested readers are addressed to related text books [11, 14].

A comparison between morphological features of image objects was done to evaluate the segmentation technique applicability. Mentioned morphological features are major axis length and minor axis length of 120 rock images that were identified based on manual segmentation and proposed segmentation technique. The mean error, the mean absolute error, the mean squared error MSE and the R^2 values were used for comparison scope. Table 2 shows the error statistics of the major and minor axis lengths for all segmentation techniques. The mean error values are 0.315 and -0.35 pixels for major and minor axis length respectively. The corresponding mean absolute error value for the technique is 16.89 and 43.31 pixels and the corresponding mean squared errors are 143.3 and 56.16.The statistical similarities between the actual values and the estimated values for the major and minor axis length were also tested for all the segmentation techniques. The t-statistics were performed for this purpose and the results are presented in Table 3. The t-statistics and their level of significance values, however, indicate that the mean values of the actual and estimated major and minor axis length are not significantly different. In view of above performance measures, it was decided that the segmentation technique is applicable to divide the individual rock samples in this case study.

After a careful examination of all the images, 405 distinct rock objects were identified. The features were then extracted from each of the individual rock objects. Altogether, 76 features were extracted. A list of the extracted features is presented in Table 5. In this table aspect ratio is described as the Major axis length divide to minor axis length. However, 76 features imposed a huge computational burden in the subsequent modeling for ore grade estimation.

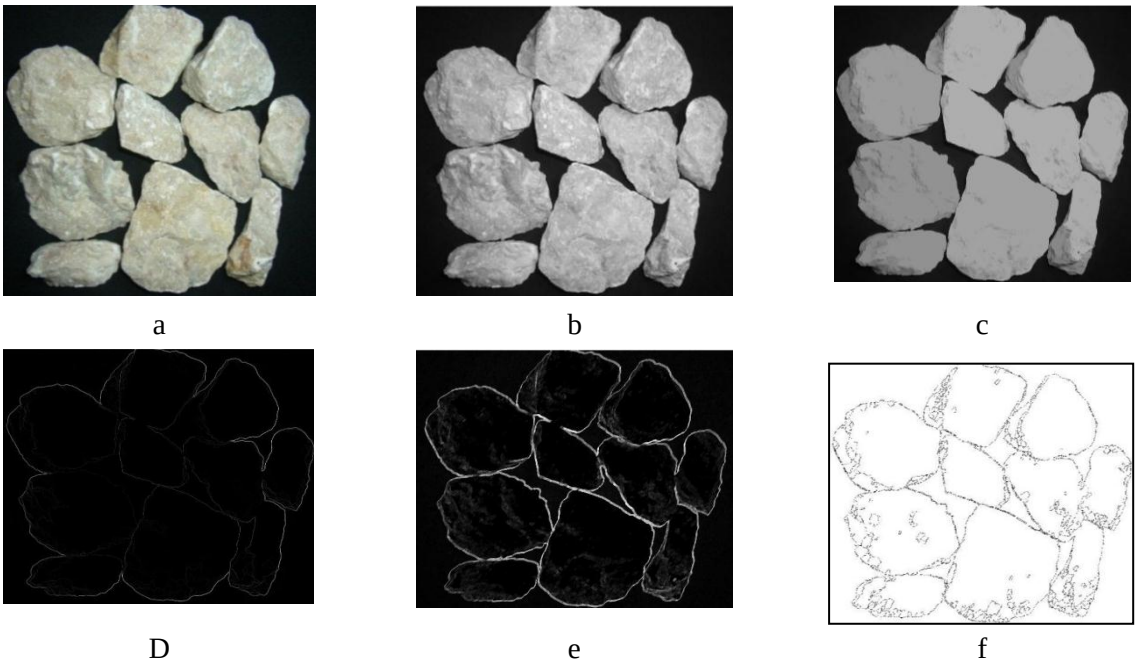

Figure 2. Sample images of different stage involved in proposed segmentation: (a) main image; (b) gray image ; (c) erosion and reconstruction transformation; (d) gradient transform; (e) dilation transform; (f) segmentation.

Table 2. Error statistics of the segmentation technique

ME		MAE		MSE	
major axis	minor axis	major axis	minor axis	major axis	minor axis
0.31	-0.35	16.89	43.31	143.32	56.16

Table 3. Paired sample t-test between manual segmentation vs. automatic segmentation

	Mean	S.D	Mean Standard Error	Critical limit		t	df	Sig
				Upper	Lower			
major axis	0.23	0.70	0.24	0.73	-0.42	0.61	119	0.23
minor axis	0.31	0.45	0.35	1.05	-0.32	0.40	119	0.31

In order to achieve the least number of features that involve most of the information, the relation between the variations of features was studied.
In this way we computed Spearman correlation coefficient for all 76 features. Considering the correlation coefficients, the features that are correlated (with a correlation coefficient greater than 0.6) are grouped and only one of them is considered for the next steps. Therefore, 17 independent features have been selected that are as follows:

- Eccentricity of the ellipse that has the same second-moments as each rock samples. The value is between 0 and 1. A rock sample with an eccentricity of 0 is actually a circle, while a rock sample whose eccentricity is 1 represents a line segment.
- Mean, variance and skewness of red component of the pixels
- range of variation for blue component that returns the difference between the maximum and the minimum amount of blue intensity for all pixels in a rock sample
- inter quartile range (IQR) of blue component, that is the difference between the 75th and the 25th percentiles of blue histogram related to rock sample
- mean, skewness and kurtosis of hue component of the pixels
- skewness of saturation component histogram
- inter quartile range of hue component histogram
- inter quartile range of saturation component histogram
- mode of saturation component histogram
- mean absolute deviation (MAD) of intensity (x) component that can be expressed as:
- MAD= mean (abs ($x_i - \overline{X}$))
- contrast and correlation and energy of the pixels as texture features. Energy indicates the set of pixels homogeneity.

The statistical parameters were computed for intensity of all pixels in a segmented rock. The variation of some statistical parameters for color component (for example IQR of red and blue and green) in different images is not interpretable and explainable. On the other hand, this variation for some statistical parameters like mean of color components for dolomite images is less than calcite images. Also the contrast, correlation and energy as texture features attempt to quantify intuitive qualities described by terms such as rough, silky, or bumpy in the context of an image. In this case, the roughness or bumpiness refers to the variations in the brightness values [11]. Al_2O_3 and Fe_2O_3 in solution phase can affect the visual features of limestone like color and subsequently the texture features of the images could be also changed.
After the extraction of features from each distinct rock object, the feature values for each of the 60 images were calculated based on the methodology that described in Section 2.1. The PCA technique was also used to reduce the dimensionality of these features. From the PCA analysis, it was noticed that 90.66% of the data variance could be explained by the first six principal components. Hence, it was decided that the first six principal components captured from the image-extracted features should be retained. Table 4 shows the amount of data variance, percentage of data variance and cumulative percentage of data variance explained by the six principal components. Figure 3 shows the percentage of variance captured by first six principal components. All PC_s are statistically independent and hence mutually orthogonal. Therefore, each PC bears independent information. The major

contributory features and their factor loadings to each of the six PC_s are as follows:

- **PC_1**: mean, kurtosis, skewness and IQR of hue, mean of red, energy
- **PC_2**: IQR of blue, MAD of intensity, skewness and variance of red, skewness and IQR of saturation, mean, IQR, range and skewness of hue, contrast, correlation
- **PC_3**: IQR and mode of saturation, IQR of blue, mean of red, skewness of hue
- **PC_4**: correlation, mode and IQR of saturation, energy, skewness of hue, IQR and range of blue, mean of red
- **PC_5**: skewness and kurtosis of hue, skewness of red, IQR of saturation, range of blue
- **PC_6**: skewness of hue, skewness and mode of saturation, contrast, mean of red

3.4. Neural network model for grade prediction

The multi-layer perceptron neural network (MLP) model was used for estimating the grades of the mineral from features. The network consisted of an input layer containing six input nodes (principal components), an output layer consisting of four output nodes corresponding to four grades attributes. The six principal components, as obtained from the PC analysis of image extracted features, were used as the input parameters and the grade attributes ($CaCO_3$, $MgCO_3$, Al_2O_3 and Fe_2O_3) were used as the output parameters of the neural network model. The grade values of these four mentioned attributes were determined following the ASTM standard [26]. The tansig activation was used both in the hidden and the output layers. The trainlm algorithm was used to train the network using the training data set. Also in order to design a generalized neural network model, in this study the model was calibrated using the early-stop training method. Early-stop training method used two data sets: (i) the training, and (ii) the calibration. The model was trained using the training data set and was calibrated using the calibration data set. However, the generalization capability of the model was tested using the testing data set. To prepare these three data sets, all of the data available to the neural network modeling was divided into the three data sets. For this purpose, images were randomly picked up and assigned to each of the three data sets in the proportion of 70:15:15 for training, calibration and testing sets. Thus, 41 images were chosen for training, 9 images for calibration, and the remaining 9 images for testing.

The quality of this random data division was tested by checking the statistical similarity among the three data subsets for all the input and the output parameters. To this end, the ANOVA F-test was performed to check the statistical similarities in mean values of the parameters for all the three data sets. The Levene statistics were also performed for the test of homogeneity of the variance [27]. The results of the statistical tests and their value of significance show that the mean and variance values of the parameters for the three data sets are not significantly different from each other. Therefore three data sets are reliable for ore grade modeling. Another important decision for neural network modeling was the selection of the number of hidden nodes and the learning parameters. The optimal number of the hidden nodes was manually determined by observing the mean squared errors of the model vs. the number of the hidden nodes. The results show that eight nodes in the hidden layer produce the minimum mean squared error in the training data set.

After model development the generalization capability of the model was examined using the testing data set. The error statistics of the observed values and the model estimated values for the three data sets are presented in Table 6.

The R^2 values for the test data are 0.78, 0.76, 0.76 and 0.81 for the grade attributes $CaCO_3$, $MgCO_3$, Al_2O_3 and Fe_2O_3 respectively. The magnitude of the coefficient of determination (R^2) indicates the correlation between actual and estimated data. Therefore, it can be inferred that the model can satisfactorily estimate the mentioned chemical compositions of the limestone.

Figure 4 (a–d) shows the scatter plots of the observed vs. model estimated values for all the four attributes. Regression lines were fitted for the observed vs. estimated values using the least square method, as can be seen in the figures. The high value of r-square in these plots show that there is high correlation between estimated and real values. A proper code for the estimation of grade and another one for image segmentation were written in (MATLAB 2009.a) software.

4. Conclusion

In this paper an image-based system was developed for grade estimation of rock samples with respect to their images features. The samples were collected from different parts of the studied mine. The images of each sample were captured, segmented and features were extracted from the segmented images. A total number of 76 features were extracted from the segmented rock samples. PCA was performed to reduce the dimension of features. Ultimately, six principal components were used for the grade determination from the

images using the neural network technique. The applicability of the designed model was tested using a testing data set at the model creation phase. The testing results show that the model was a good estimator for four grade attributes. The designed model is not applicable to other minerals directly. Before applying the model to other deposits, the neural network model must be trained with rock samples from that same deposit, and same type of image acquisition set up must be used.

References

[1] Malamas, M., Elias, N., Petrakis, E.G.M., Zervakis, M., Petit, L. and Legat Jean-Didier. (2003). A survey on industrial vision systems, applications and tools, Image Vision Computing, 21 (2): 171–188.

[2] Oestreich, J., Tolley, W. and Rice, D. (1995). The development of a color sensor system to measure mineral compositions, Minerals Engineering, 8 (l/2): 31–39.

[3] Petruck, W. and Lastra, R. (1993). Evaluation of recovery of liberated and unliberated chalcopyrite by flotation columns in a copper cleaner circuit, International Journal of Mineral Processing, 40 (1–2): 137–149.

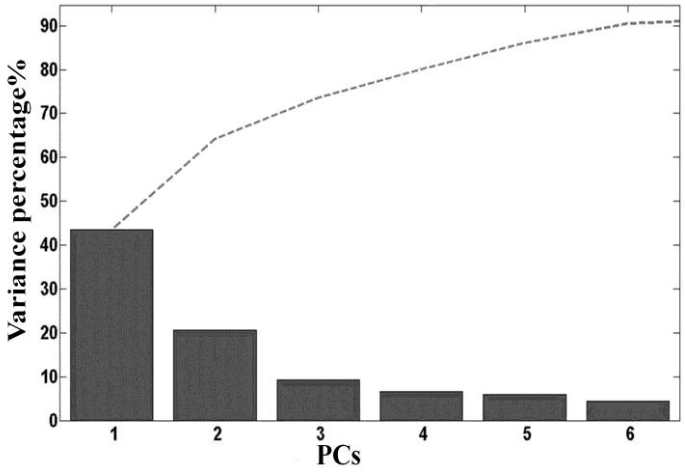

Figure 3. Percentage of data variance captured by six principal components

Table 4. Captured variance by first six principal components

Principal component	PC_1	PC_2	PC_3	PC_4	PC_5	PC_6
Data variance captured	0.35	0.16	0.07	0.05	0.04	0.03
Percentage of data variance (%)	43.60	20.63	9.38	6.69	5.88	4.48
Cumulative percentage of data Variance (%)	43.54	64.17	73.49	80.12	86	90.66

Table 5. The number of extracted features from segmented rock samples

Morphological feature	Textural feature (co-occurrence matrix)	Color feature	Color feature
major axis length (1)	contrast (4)	kurtosis (7)	mean (7)
minor axis length (1)	correlation (4)	IQR (7)	mode (7)
aspect ratio (1)	energy (4)	MAD (7)	variance (7)
eccentricity (1)	homogeneity (4)	range (7)	skewness (7)

Table .6 Error statistics for different data set

	Training Data set		Calibration Data set		Testing Data set	
Component	RMSE	R^2	RMSE	R^2	RMSE	R^2
$CaCO_3$	0.8	0.88	0.72	0.81	0.38	0.78
$MgCO_3$	0.85	0.82	0.02	0.74	0.84	0.76
Al_2O_3	0.12	0.79	0.13	0.75	0.15	0.76
Fe_2O_3	0.03	0.83	0.03	0.78	0.03	0.81

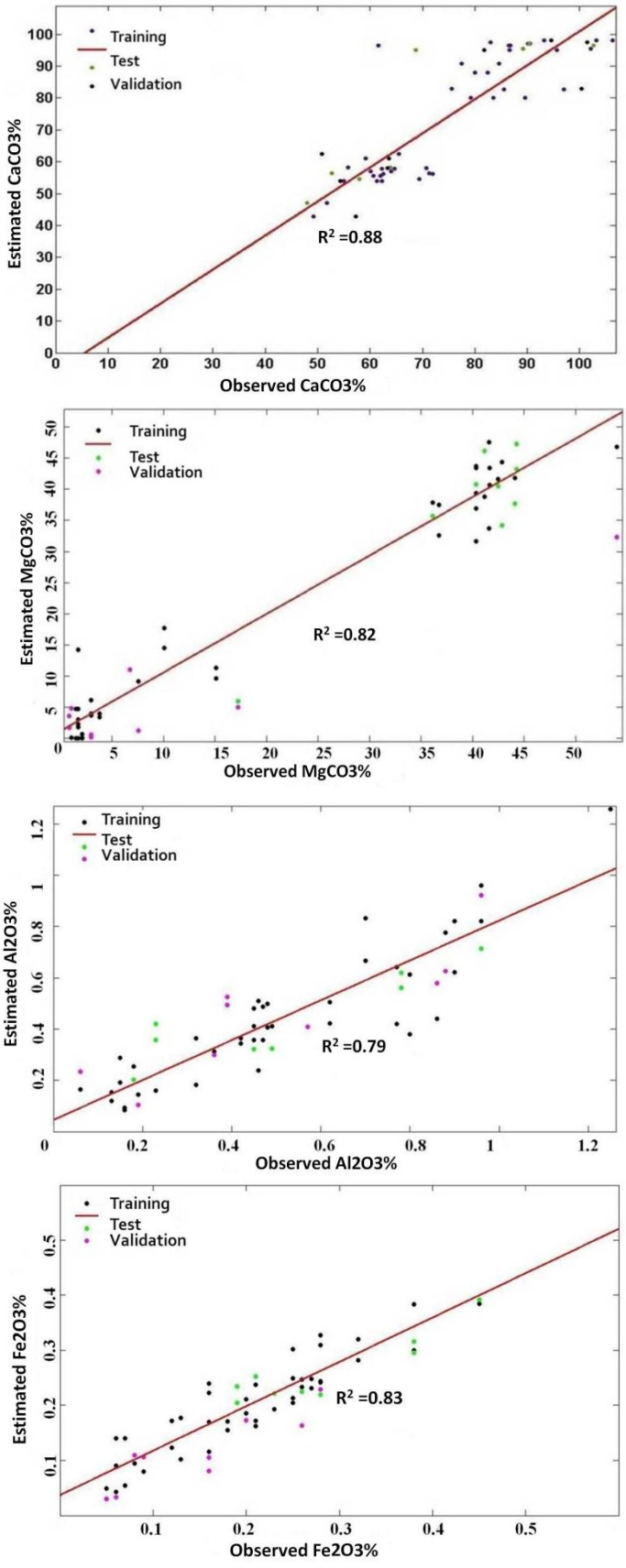

Figure 4. Scatter plot of observed vs. estimated value of four attributes using neural regression: (a) $CaCO_3$; (b) $MgCO_3$; (c) Al_2O_3; (d) Fe_2O_3.

[4] Shafarenko, L., Petrou, M. and Kittler, J. (1997). Histogram-based segmentation in a perceptually uniform color space, IEEE Transactions on Image Processing, 7 (9): 1354–1358.

[5] Casali, G., Vallebuona, C., Pe´ rez, G., Gonza´ lez, R. and Vargas, L. (2000). Lithological composition and ore grindability sensors, based on image analysis, in: Proceedings of the XXI IMPC, Rome: 9–16.

[6] Petersen, K.R.P., Aldrich, C. and Vandeventer, J.S.J. (1998). Analysis of ore particles based on textural pattern recognition, Minerals Engineering, 11 (10): 959–977.

[7] Henley, K.J. (1983). Ore-dressing mineralogy—a review of techniques, applications and recent developments, Special Publication-Geological Society of South Africa, 7(2): 175–200.

[8] Jones, M.P. and Horton, R. (1979). Recent development in the stereological assessment of composite (middlings) particles by linear measurements, in: M.J. Jones (Ed.), Proceedings of the XIth Commonwealth Mining and Metallurgical Congress, IMM, London: 113–122.

[9] Lin, C.L., Yen, Y.K. and Miller, J.D. (1993). Evaluation of a PC image-based on-line coarse particle size analyzer, in: Proceedings of Emerging Computer Techniques for the Mineral Industry Symposium, AIME/SME, 201–210.

[10] Chatterjee, S., (2006). Geostatistical and image based quality control models for Indian mineral industry. un published Ph.D. Thesis dissertation, IIT Kharagour, India, 272pp.

[11] Gonzalez, R.C. and Woods, R.E. (2002). Digital image processing, Prentice-Hall, NJ, USA, 793pp.

[12] Parker, J.R. (1993). Practical computer vision using C, John Wiley and Sons Inc., New York, NY, 476 pp.

[13] Perez, A. and Gonzalez, R.C. (1987). An iterative thresholding algorithm for image segmentation, IEEE Transaction on Pattern Analysis and Machine Intelligence 9 (6): 742–751.

[14] Jain, A.K. (1995). Fundamental of digital image processing, Prentice-Hall of India Pvt. Ltd, New Delhi, India, 569pp.

[15] Graham, D.J., Reid, I. and Rice, S.P. (2005). Automated sizing of coarse-grained sediments: image-processing procedures, Mathematical Geology, 37 (1): 1–28.

[16] Haralick, R.M. and Shapiro, L.G. (1992). Computer and robot vision 1 & 2, Addison-Wesley, Reading, MA, 630 pp.

[17] Kim, T.H., Cho, T.H., Moon, Y.S. and Park, S.H. (1999). Visual inspection system for the classification of solder joints, Pattern Recognition, 32 (4): 565–575.

[18] Flugel, E. (2004). Microfacies of Carbonate Rocks: Analysis Interpretation and Application, Springer, NY, USA, 976 pp.

[19] Haralick, R.M. and Shanmugam, I., K.S. (1973). Dinstein, Textural features for image classification, IEEE Transactions on Systems, Man, and Cybernetics, 3 (6): 610–621.

[20] Zucker, S.W. and Terzopoulos, D. (1980). Finding structure in co-occurrence matrices for texture analysis, Computer Graphics and Image Processing, 12 (3): 286–308.

[21] Hamid, M.H. (2001). Feature vector based analysis: a unified concept for multivariate image analysis, in: Irish Machine Vision and Image Processing Conference (IMVIP 2001), Ireland, NUI Maynooth, 219–226.

[22] Jolliffe, I.T. (1986). Principal component analysis, Springer-Verlag, NY, USA, 487 pp.

[23] Haykins, S. (1998). Neural networks: a comprehensive foundation, Prentice-Hall, NJ, 842 pp.

[24] Bishop, C.M. (1996). Neural network for pattern recognition, Oxford University Press, USA, 504 pp.

[25] Hagan, M.T., Demuth, H.B. and Beale, M. (1995). Neural network design, PWS Publishing Company, Boston, 736 pp.

[26] http://www.astm.org/Standards/C25.html

[27] Olkin, I., Ghurye, S.G., Hoeffding, W., Madow, W.G. and Mann, H.B. (1960). Contributions to probability and statistics: essays in honor of harold hotelling, Stanford University Press, 520 pp.